Langmuir

Article

pubs.acs.org/Langmuir

Polyvinylferrocene for Noncovalent Dispersion and Redox-Controlled Precipitation of Carbon Nanotubes in Nonaqueous Media

Xianwen Mao, Gregory C. Rutledge,* and T. Alan Hatton*

Department of Chemical Engineering, Massachusetts Institute of Technology, 77 Massachusetts Avenue, Cambridge, Massachusetts 02139, United States

Supporting Information

ABSTRACT: We report noncovalent dispersion of carbon nanotubes (CNTs) in organic liquids with extremely high loading (~2 mg mL^{-1}) using polyvinylferrocene (PVF). In contrast to common dispersants, PVF does not contain any conjugated structures or ionic moieties. PVF is also shown to be effective in controlling nanotube dispersion and reprecipitation because it exhibits redox-switchable affinity for solvents, while maintaining stable physical attachment to CNTs during redox transformation. This switchability provides a novel approach to creating CNT-functionalized surfaces. The material systems described here offer new opportunities for applications of CNTs in nonaqueous media, such as nanotube−polymer composites and organic liquid-based optical limiters, and expand the means of tailoring nanotube dispersion behavior via external stimuli, with potential applications in switching devices. The PVF/CNT hybrid system with enhanced redox response of ferrocene may also find applications in high-performance biosensors and pseudocapacitors.

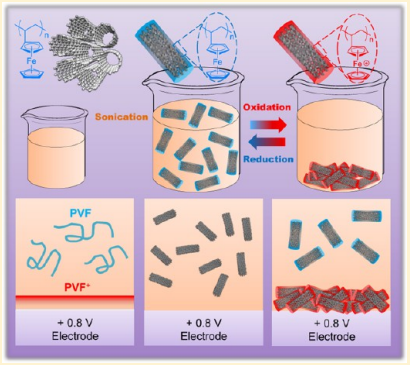

INTRODUCTION

Effective dispersion of carbon nanotubes (CNTs) in solvents and polymer matrices remains a major challenge for both fundamental research and practical applications since pristine nanotubes form large bundles due to strong van der Waals interactions.[1−4] The common strategies to disperse CNTs fall into two general categories: chemical functionalization and noncovalent surface modification.[4] Chemical treatment inevitably involves disruption of the long-range π conjugation of the nanotube, leading to partial loss of electronic properties and mechanical strength. Therefore, the noncovalent approach is considered advantageous in that it maintains the sp^2-conjugated structures of CNTs and therefore preserves their intrinsic properties and performance.

Exploring new chemical structures that can *noncovalently* disperse pristine carbon nanotubes is of immense significance, since it allows niche design of a great variety of novel dispersants to extend and diversify applications of CNTs in various media. Chemical moieties commonly employed to disperse CNTs based on noncovalent interactions include nucleotide bases,[5−8] pyrenes,[9−11] porphyrins,[12−14] and long-range conjugated polymeric structures such as poly(3-alkylthiophene),[15−18] poly(*m*-phenylenevinylene),[19,20] and poly(arylene ethynylene).[21,22] Noncovalent dispersion of CNTs in water dominates the literature,[4] mainly because common dispersants contain large, rigid conjugated structures and/or ionic moieties. Conjugated structures typically have solubility or miscibility issues in organic solvents due to strong interchain $\pi-\pi$ interactions,[23] while ionic moieties give rise to a high level of hydrophilicity and thus low solubility in nonaqueous media. Therefore, highly effective dispersion of CNTs in nonaqueous media remains a great challenge; the CNT concentrations achieved in organic liquids using non-covalent-type dispersants are generally less than 0.1 mg mL^{-1}.[24−30] The dispersion efficiency of nanotubes in organic solvents has been improved by introducing an unconjugated segment to a conjugated polymer to increase its solubility in organic solvents[23] and by using a phase transfer catalyst to dissolve a hydrophilic ionic dispersant in nonaqueous media.[31] Still, there exists no general chemical structure that can noncovalently disperse CNTs with high loading in organic solvents.

Furthermore, there has been growing interest in stimuli-responsive CNT dispersants for regulating dispersion and aggregation of nanotubes in solvents in order to develop nanotube-based responsive systems such as switching devices and sensors. Noncovalent-type dispersants that respond to light,[32] pH,[33−35] temperature,[35,36] CO_2,[37] and solvent polarity[28] have been reported. To achieve highly effective control over dispersion and aggregation of nanotubes in solvents, the desired dispersant should exhibit remarkable change of affinity for solvents upon application of stimuli, while maintaining stable attachment to CNTs. For instance, poly(*N*-isopropylacrylamide) is a well-known thermoresponsive polymer;[38] however, its physical interaction with CNTs is weak and not sufficient for effective stabilization of CNTs and/or control over their dispersion state.[35] In contrast, pyrene-functionalized poly(*N*-cyclopropylacrylamide) (p-PNCPA) shows an improved ability

Received: April 16, 2013
Revised: June 21, 2013
Published: June 25, 2013

   dx.doi.org/10.1021/la401440w | Langmuir 2013, 29, 9626−9634

to manipulate the dispersion state of CNTs by temperature since the PNCPA backbones exhibit thermoresponsive affinity for the solvent, while the pyrene side groups can attach stably to the nanotube surface during the temperature-induced transition.[36] However, few attempts have been made to regulate the dispersion and aggregation behavior of CNTs using redox-responsive systems, possibly due to lack of redox moieties that exhibit strong noncovalent interactions with CNTs.

Here we report a redox-responsive, unconjugated, nonionic polymer, polyvinylferrocene (PVF) that can noncovalently disperse pristine carbon nanotubes in organic solvents to a high degree, generating fully exfoliated CNT dispersions composed largely of individualized tubes and with extremely high nanotube solubility (~2 mg mL^{-1}). We also demonstrate that PVF is highly effective in controlling nanotube dispersion and aggregation because of its dual ability to exhibit dramatic affinity change for organic solvents in response to redox stimuli[39] as well as to maintain stable physical attachment to CNTs during redox transformation. Covalent functionalization of CNTs by ferrocene derivatives has been reported;[40−43] however, there is no study dealing with noncovalent dispersion of pristine CNTs using ferrocene. Although physical mixtures of ferrocene and CNTs have been prepared and used for electrochemical sensing,[44−47] it is not clear that efficient noncovalent dispersion of pristine CNTs by ferrocene was achieved in these reports. First, before mixing with ferrocene, the CNTs were subject to harsh acid treatment,[44−47] which may already have disrupted seriously the sp^2-conjuagated structures of the nanotubes. Therefore, these preparation methods failed to preserve the intrinsic properties of pristine nanotubes. Second, the ability of ferrocene to disperse nanotubes was not demonstrated unambiguously. In the work by Huang et al.,[44] the CNT suspension was obtained at a very low concentration (~10^{-5} mg mL^{-1}, which is 10^5 times lower than the value we have obtained); at such a low concentration, the acid-treated CNTs may be dispersed merely by sonication without ferrocene as the dispersant. Also, the CNT suspension obtained in that study consisted of large nanotube bundles, indicating poor dispersion quality; in contrast, our work shows that PVF can disperse untreated, pristine CNTs into individualized tubes. In the other three reports,[45−47] the ferrocene/CNT hybrid was merely a solid mixture of the two components, and no stable CNT dispersion was ever obtained. Therefore, our work provides the first experimental evidence that ferrocene-containing molecular systems can noncovalently disperse pristine carbon nanotubes with high efficiency.

Our study points to a new direction for the development of next-generation noncovalent-type dispersants that do not rely on any conjugated or ionic structures, since ferrocene moieties can be easily introduced to a variety of surfactants and polymers via facile synthetic protocols. This work also indicates a number of exciting, distinct functions of PVF for expanding CNT technologies that may be unattainable with previously reported dispersants. First, in contrast to most water-based dispersants, PVF can disperse large amounts of CNTs in organic solvents with excellent dispersion quality. This is useful for realizing high CNT loading in polymers (e.g., polystyrene[48]), processing of which is often carried out in nonaqueous media, and for producing high-concentration nanotube dispersions in organic liquids for the design of CNT-based switchers, mode lockers, and optical limiters.[49] Second, PVF's redox responsiveness allows for controlling dispersion and aggregation of nanotubes in organic solvents, which cannot be achieved using most stimuli-responsive dispersants due to their hydrophilicity; these include lysozyme,[34] poly(acrylic acid),[33] poly(*N*-isopropylacrylamide),[35] poly(L-lysine),[35] pyrene-functionalized poly(*N*-cyclopropylacrylamide),[36] poly(ethylene glycol)-terminated malachite green,[32] and a pyrene-containing amidinium cation.[37] More interestingly, unlike other types of stimuli (e.g., pH, temperature, light, and solvent polarity), redox stimuli can be effected *locally* by electrochemical methods. A localized oxidative environment created by applying a proper electrochemical potential can induce deposition of PVF-wrapped nanotubes to conductive substrates, and electrochemical conditions can be used to manipulate this surface modification process. This provides a novel and controllable approach to creating CNT-functionalized surfaces with many potential applications such as nanotube-based catalysis and sensing. Third, combining conductive CNTs with PVF can facilitate electron transport in the polymer/nanotube hybrid system, leading to efficient utilization of ferrocene moieties with enhanced current response. Since ferrocene can undergo reversible and fast redox reactions and functions as a redox mediator for enzymes, the PVF/CNT hybrid may contribute to the development of high-performance pseudocapacitors and biosensors, respectively.

EXPERIMENTAL SECTION

Materials. Polyvinylferrocene (PVF, molecular weight = 50 000 g mol^{-1}) was obtained from Polysciences and used as received. Multiwalled carbon nanotubes (MWCNTs) with a diameter of 6−9 nm and purity of 95% and single-walled carbon nanotubes (SWCNTs) with a diameter of 1.2−1.5 nm and purity of 70% were obtained from Sigma-Aldrich and were used as received throughout the study, without further purification or modification unless otherwise noted.

Characterization. Transmission electron microscopy (TEM) images were taken using a JEOL-2010 TEM. Atomic force microscopy (AFM) images were taken with a Veeco Nanoscope V AFM with Dimension 3100 using the tapping mode in ambient air with silicon tips. The dynamic light scattering (DLS) measurement was performed using a Brookhaven BI-200SM light scattering system. Optical microscopy (OM) images were taken using a Carl Zeiss Axio Observer. Fourier transform infrared (FTIR) measurements were performed on a Nicolet Nexus 870 ESP spectrometer. X-ray photoelectron spectra (XPS) were recorded with a Kratos Axis Ultra instrument equipped with a monochromatic Al Kα source operated at 150 W. Scanning electron microscopy (SEM) images were taken using a Zeiss Supra-40 SEM. A HORIBA Jobin Yvon Labram HR800 spectrometer was used for recording the Raman spectra using a 633 nm laser source. Thermogravimetric analysis (TGA) experiments were carried out using a TA Q50 instrument. UV−vis absorption spectra were obtained using a Hewlet-Packard 8453 spectrophotometer. Electrochemical experiments were performed using an AutoLab PGSTAT 30 potentiostat with GPES software.

Additional experimental details are provided in the Supporting Information.

RESULTS AND DISCUSSION

Dispersion Efficiency of CNTs by PVF. With a PVF/CNT mass ratio of 2:1, stable CNT dispersions in chloroform were achieved readily via gentle bath sonication (VWR Scientific Model 75T Aquasonic, power ~ 90 W, frequency ~ 40 kHz) for 45 min at 0 °C without any pretreatment of the pristine nanotubes. Transmission electron microscopy (TEM) was used to examine the dispersion quality of CNTs by PVF in solution. The TEM image of a PVF/multiwalled CNT (MWCNT) dispersion (Figure 1a) shows that the majority of

dx.doi.org/10.1021/la401440w | *Langmuir* 2013, 29, 9626−9634

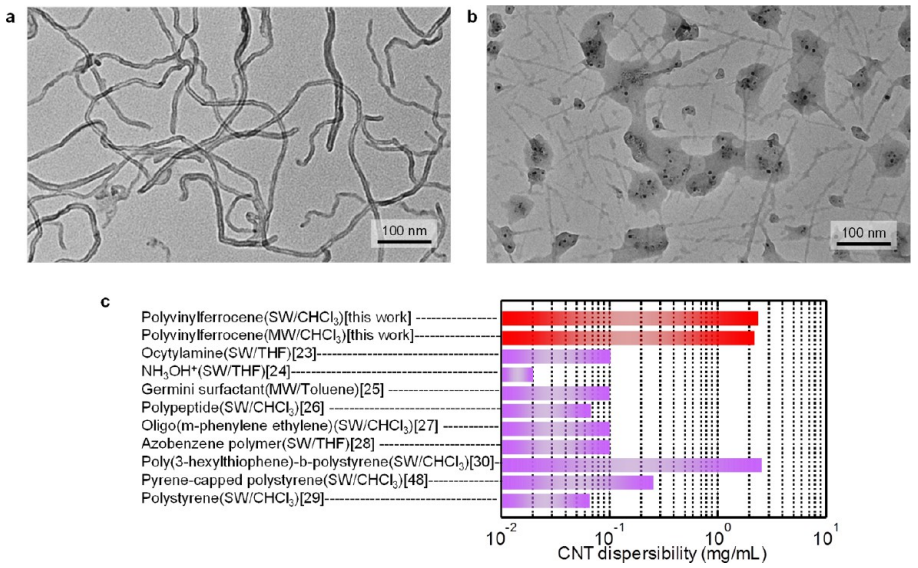

Figure 1. Dispersion of CNTs by PVF. (a, b) TEM images of (a) a PVF/MWCNT dispersion and (b) a PVF/SWCNT dispersion. The PVF/CNT mass ratio in both cases is 2:1. (c) Comparison of CNT dispersibility in organic solvents using various noncovalent-type dispersants.

MWCNTs were debundled individual nanotubes. As for the PVF/single-walled CNT (SWCNT) dispersion, the major component (Figure 1b) is believed to be completely debundled nanotubes with an average diameter around 2−5 nm, coexisting with another group of slightly bundled SWCNTs with an average diameter around 10−12 nm. Moreover, the CNT loadings obtained by using PVF as the dispersant (2.3 ± 0.1 mg mL^{-1} for SWCNTs and 2.2 ± 0.1 mg mL^{-1} for MWCNTs) exceeded significantly most of the reported values for CNT dispersions in organic solvents using other noncovalent-type dispersants[23−30,48] (Figure 1c). The method of determining the CNT solubility is presented in the Supporting Information (SI) section S1.1. The PVF/CNT dispersions exhibited excellent long-term stability with negligible concentration change of dispersed nanotubes after 4 months standing at room temperature. This stability was monitored by light absorbance of the dispersions (for experimental details, see SI section S1.2). It should be noted that similar dispersion quality and stability can be obtained using mass ratios of PVF to CNT higher than 0.2. We also demonstrate that the dispersion quality of CNTs in a hydrophobic polymer matrix, polystyrene, was improved through using PVF as the dispersant (SI section S2). This is of great interest since the performance and function of CNT−polymer composites depend strongly upon the dispersibility of the nanotubes in polymer media.[1,4,23,48,50]

Noncovalent Functionalization of CNTs by PVF. The PVF-modified CNTs were prepared by multiple cycles of sonication and centrifugation of the PVF/CNT dispersion to remove the unadsorbed polymers until no PVF was detectable by UV−vis spectroscopy in the supernatant (for experimental details, see SI section S1.4). Some representative high-resolution TEM (HR-TEM) images of PVF-modified MWCNTs (Figure 2a) reveal clearly the presence of self-assembled ferrocene clusters with an average diameter around 2 nm on the nanotube surfaces, indicating effective surface functionalization of CNTs by PVF. In contrast, the pristine MWCNTs (Figure 2b) exhibited clean surfaces. We suspect that multiple polymer chains adsorbed to one single MWCNT, possibly because PVF, which has a hydrodynamic diameter of 7.4 nm in chloroform (as determined by dynamic light scattering (DLS), see SI section S1.5), is not sufficiently long to wrap around one nanotube. Atomic force microscopy (AFM)-based phase imaging in air is a powerful tool to elucidate variations in material properties such as adhesion, friction, and viscoelasticity and therefore can be used to distinguish between different materials. The AFM phase image of a PVF-modified MWCNT (Figure 2c) shows that it displayed a somewhat undulated surface with remarkable phase variations at several selected locations along the length of the nanotube. In contrast, the as-received MWCNTs (Figure 2d) had smooth surfaces with flat phase profiles. This suggests that the nanotube surface in the former case was covered by a different type of material, most likely the polymers. AFM images of the deposited films prepared from pure PVF, as-received MWCNTs, and PVF-modified MWCNTs are shown in Figure S11. The PVF film exhibited a flat topology whereas in the latter two cases interconnected carbon nanotubes could be clearly observed. Also, the diameters of the neat carbon nanotubes were smaller than those of the PVF-modified CNTs, due to surface functionalization of the nanotubes by the polymer. The Fourier transform infrared (FTIR) spectra of PVF-modified MWCNTs (Figure 2e) and SWCNTs (Figure 2f) showed characteristic ferrocene peaks around 1105, 1022, 1001, and 801 cm^{-1}.[51] As a control, the FTIR spectrum for PVF is shown in Figure S10. High-resolution Fe 2p X-ray photoelectron spectra (XPS) for PVF-modified MWCNTs (Figure 2g) and SWCNTs (Figure 2h) exhibited two bands around 721 and 708 eV, corresponding to the Fe $2p_{1/2}$ and Fe $2p_{3/2}$ orbitals, respectively. Moreover, based on quantitative analyses of the XPS survey scans (see SI section S1.6), the Fe/C ratio (atom %) was 0.5% for PVF-modified SWCNTs, 0.9% for PVF-modified MWCNTs, and 2.1% for pure PVF. The Fe content was zero for as-received SWCNTs and MWCNTs based on their XPS survey scans. This indicates that the iron signals of the PVF-modified carbon nanotubes resulted solely from the ferrocene molecules, not from traces of metallic impurities possibly present in the CNT samples. The FTIR and XPS analyses confirm the presence of ferrocene molecules in the PVF-modified CNTs, indicating that PVF was attached to both SWCNTs and MWCNTs.

dx.doi.org/10.1021/la401440w | Langmuir 2013, 29, 9626−9634

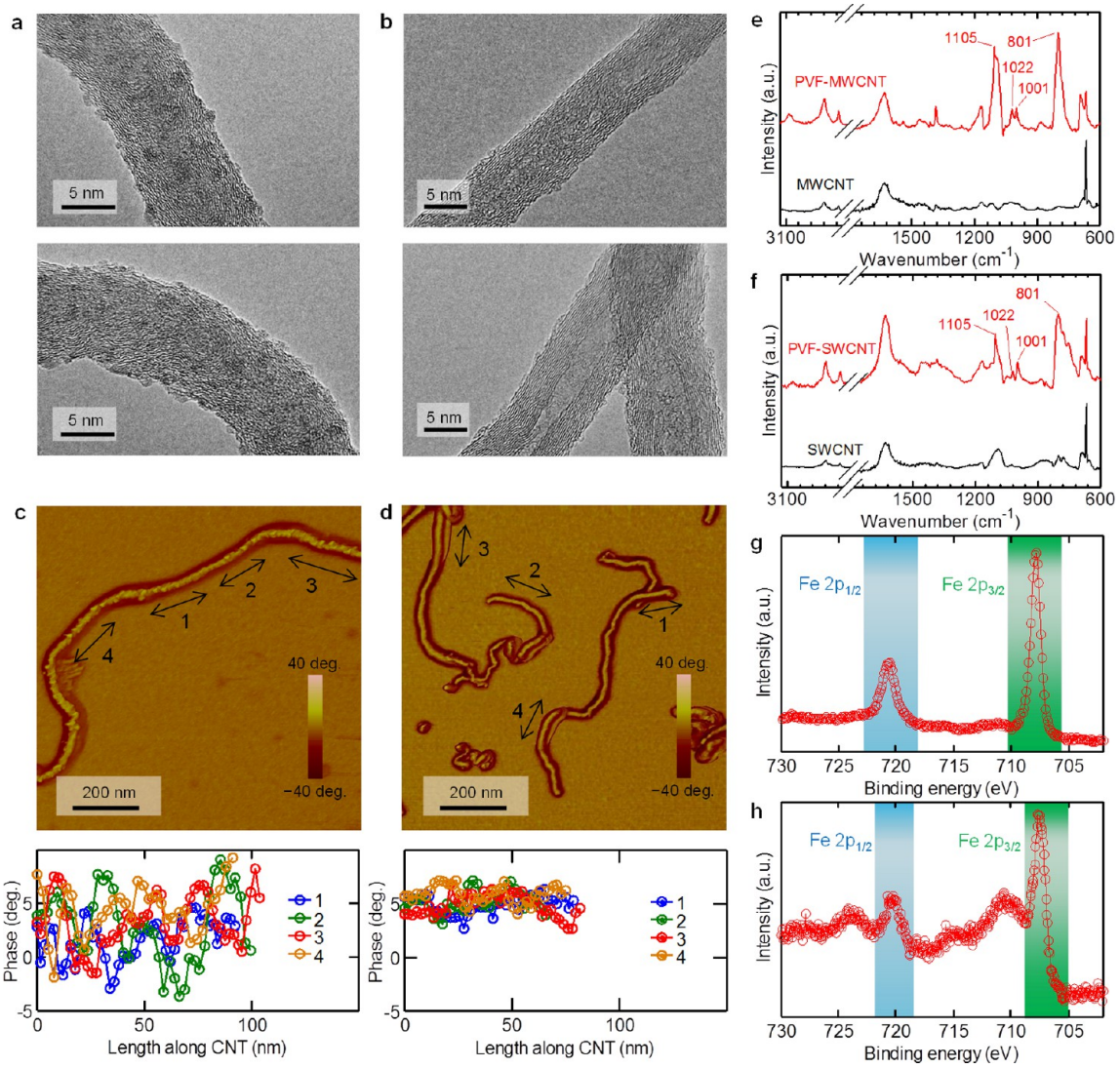

Figure 2. Noncovalent functionalization of CNTs by PVF. (a, b) HR-TEM images of (a) PVF-modified MWCNTs and (b) untreated MWCNTs, showing the self-assembled ferrocene clusters on the nanotube surface in the former case. (c, d) AFM phase images of (c) a PVF-modified MWCNT and (d) untreated MWCNTs, together with the phase profiles of the marked locations, showing the difference in phase variation between the two cases. (e, f) FTIR spectra of (e) PVF-modified MWCNTs and untreated MWCNTs, (f) PVF-modified SWCNTs and untreated SWCNTs. (g, h) High-resolution XPS Fe 2p spectra for (g) PVF-modified MWCNTs and (h) PVF-modified SWCNTs.

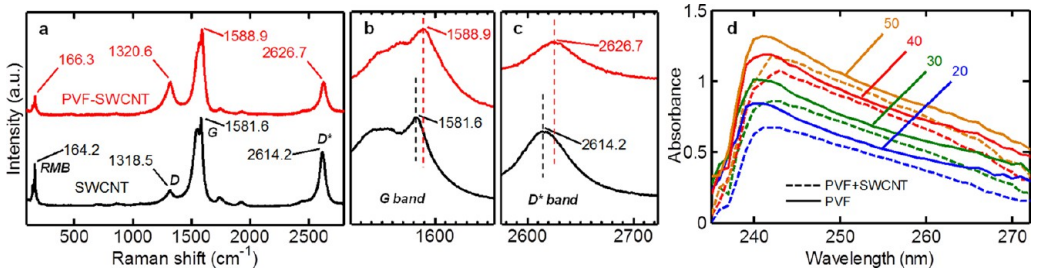

Figure 3. Molecular-level interactions between PVF and CNTs. (a) Raman spectra of pristine SWCNTs and PVF-modified SWCNTs. Magnifications of the G and D* bands are shown in (b) and (c), respectively, showing the significant upshifts of the maxima of the G and D* bands of the SWCNTs after treatment with PVF. (d) Energy absorption bands from the $\pi \rightarrow \pi^*$ transition of the cyclopentadiene rings of PVF for the reference samples (solid lines) and the CNT-containing samples (dashed lines) showing the suppression of the energy bands when SWCNTs were present. The reference sample and the CNT-containing sample labeled by the same color contain the same PVF concentration. The numbers with different colors indicate the concentrations of PVF in units of μg mL^{-1}. The concentrations of SWCNTs in the CNT-containing samples were 5 μg mL^{-1}.

Molecular-Level Interactions between PVF and CNTs. Raman spectroscopy was used to assess the electronic structure of CNTs before and after functionalization with PVF. The characteristic Raman bands of as-received SWCNTs and PVF-

dx.doi.org/10.1021/la401440w | Langmuir 2013, 29, 9626−9634

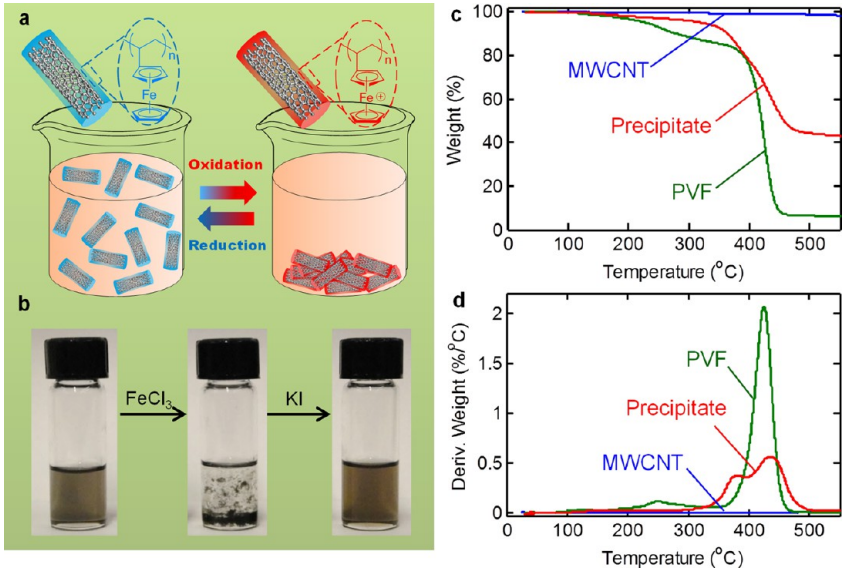

Figure 4. Redox-controlled dispersion and precipitation of CNTs using PVF. (a) Conceptual illustration of the redox-controlled dispersion and precipitation of the PVF/CNT complexes based on PVF's switchable affinity for the solvent. Blue and red colors indicate the reduced and oxidized state of PVF, respectively. (b) Photographs of a PVF/MWCNT dispersion, the same dispersion after addition of $FeCl_3$, showing the precipitated nanotubes, and the same dispersion after addition of KI followed by 5 min sonication, showing the redispersed nanotubes. (c) TGA curves and (d) differential TGA curves for untreated MWCNTs (blue), pure PVF (green), and the precipitate from oxidation of the PVF/CNT dispersion (red).

modified SWCNTs are shown in Figure 3a, from which we observed that, after treatment with PVF, the tangential vibrational mode (G band) and the second disordered band (D* band) of SWCNTs upshifted significantly from 1581.6 to 1588.9 cm^{-1} and from 2614.2 to 2626.7 cm^{-1}, respectively (also see Figure 3b,c), while the radial breathing modes (RBM) and the first disordered band (D band) shifted slightly from 164.2 to 166.3 cm^{-1} and from 1318.5 to 1320.6 cm^{-1}, respectively. Similar upshifts have also been observed in other SWCNT/dispersant systems and attributed to the molecular-level charge-transfer interactions between SWCNTs and dispersants.[23,48,52]

The $\pi-\pi$ stacking interactions between the cyclopentadiene rings of PVF and the nanotube surfaces were probed by UV–vis spectroscopy for the change of the energy absorption of PVF after interacting with SWCNTs in solution, based on the procedure proposed by Costanzo et al.[53] (for details, see SI section 1.7). PVF has a characteristic energy absorption band around 240 nm that corresponds to the $\pi \rightarrow \pi^*$ transition of the cyclopentadiene ring of the ferrocene molecule.[54] We expect to see a change in the intensity of this band if the π-electrons of the cyclopentadiene rings interact with the π-conjugated CNT surfaces. To examine the energy absorption change, two different kinds of samples were prepared: (1) four samples in which only PVF was dissolved in tetrahydrofuran (THF) at concentrations of 20, 30, 40, and 50 $\mu g\ mL^{-1}$ (named, reference samples); (2) another four samples in which a fixed quantity of SWCNTs (5 $\mu g\ mL^{-1}$) was present while the polymer concentrations were kept the same as the reference samples (i.e., 20, 30, 40, and 50 $\mu g\ mL^{-1}$). The absorption spectra of the four reference samples and the four SWCNT-containing samples are shown in Figure 3d. The intensities of the $\pi \rightarrow \pi^*$ transition bands of the CNT-containing samples are suppressed remarkably relative to those of the reference samples, indicating strong $\pi-\pi$ stacking interactions between the π-electron-rich cyclopentadiene rings of PVF and the CNTs.

Redox-Controlled Dispersion and Precipitation of CNTs Using PVF. Previous work in our group has shown that the affinity of ferrocene moieties for organic solvents is reduced significantly upon oxidation to ferrocenium ions.[39] Therefore, we expect that well-dispersed PVF/CNT complexes in chloroform will become solvophobic upon oxidation of ferrocene, leading to coprecipitation of polyvinylferrocenium (PVF^+) and carbon nanotubes. Since ferrocene can undergo highly reversible and fast redox reactions, with both the reduced and oxidized forms being chemically stable,[55,56] we can take advantage of this behavior to manipulate reversibly the dispersion and precipitation of the PVF/CNT complexes. The redox-controlled dispersion/precipitation process is illustrated schematically in Figure 4a. We also demonstrate the ability of PVF to maintain stable attachment to the nanotubes during redox transformation by applying electrochemical stimuli.

We found that PVF exhibited switchable affinity for chloroform through the use of $FeCl_3$ and KI[57] to oxidize and reduce, respectively, the ferrocene moieties (see SI section S3). On the basis of this behavior, we used the same redox stimuli to regulate the dispersion and precipitation of the PVF/CNT complexes in chloroform (Figure 4b). Well-dispersed PVF/MWCNT complexes (0.01 mg mL^{-1}, PVF:CNT = 1:1 by mass) in chloroform precipitated out immediately upon addition of an equimolar amount of $FeCl_3$ with respect to ferrocene. The weight loss of this precipitate during thermogravimetric analysis (TGA, Figure 4c) was 57% at 550 °C, whereas the weight losses of untreated MWCNTs and pure PVF under the same experimental conditions were 1% and 92%, respectively. The TGA results indicate that the PVF/CNT ratio in the precipitate was about 1:1 (w/w). This ratio is consistent with the initial composition of the dispersion, confirming complete coprecipitation of CNTs and PVF upon oxidation. Differential TGA curves are displayed in Figure 4d. The neat PVF exhibited a slight weight loss step at 246 °C and a more significant weight loss step at 424 °C, in accordance

dx.doi.org/10.1021/la401440w | Langmuir 2013, 29, 9626–9634

with previous investigations.[58] The two changes in weight for the PVF/CNT precipitate occurred at 378 and 437 °C. The first peak for the precipitate at 378 °C may be attributed to the loss of the anion (i.e., Cl^-). This explains the observation that the weight loss of the precipitate (58%) was slightly larger than half the weight loss value of the pure PVF sample (92%/2 = 46%). The second peak at 437 °C is probably due to PVF decomposition. This decomposition temperature is upshifted slightly compared to that for the pure PVF (424 °C). This may be ascribed to the interaction between PVF and CNTs. Sonication alone was insufficient to redisperse the aggregated CNTs. Addition of an equimolar amount of KI to reduce PVF^+, followed by sonication for 5 min, resulted in well-dispersed PVF/CNT complexes again (Figure 4b). The dispersion–precipitation–redispersion cycle could be repeated at least 10 times without observable changes.

To investigate whether PVF dissociates from CNTs after oxidation, the PVF/CNT complex in the dispersion was subjected to electrochemical oxidation, which can provide a localized oxidative environment on the electrode surface. A potential of 0.8 V versus Ag/AgCl (which can provide full conversion of ferrocene to ferrocenium) was applied to a carbon paper (CP) electrode that was immersed in the PVF/CNT dispersion, with 0.1 M tetrabutylammonium perchlorate (TBAP) as the background electrolyte. For comparison, electrochemical oxidation under the same experimental conditions was also performed in dispersions containing PVF alone and MWCNTs alone, respectively. Figure 5a–c gives schematic illustrations of the electrochemical oxidation processes in different dispersions and corresponding scanning electron microscopy (SEM) images of the electrode surfaces after oxidation for 30 min (higher magnification images are shown in Figure S12). See SI section S1.9 for experimental details.

When comparing the surface morphology of an untreated CP electrode (Figure S13) to that of the CP electrode treated by electrochemical oxidation in the PVF/chloroform solution (Figure 5a and Figure S12a), we observed the formation of polymer layers on the electrode surface due to the precipitation of PVF^+. This is expected because the polymer becomes solvophobic once it arrives at the electrode surface and is oxidized. The existence of PVF on the electrode surface was also verified by cyclic voltammetry (CV), as discussed later.

The fiber morphology of the CP electrode after oxidation in the MWCNT/chloroform dispersion (Figure 5b and Figure S12b) was the same as that of the pristine CP electrode (Figure S13). This suggests that MWCNTs alone could not be deposited oxidatively onto the electrode. The absence of CNTs on the electrode surface in this case was also confirmed by Raman spectroscopy, as discussed later.

When electrochemical oxidation is applied to the PVF/CNT dispersion, an important consideration is whether the CNTs can be deposited together with their polymer shells. If PVF were detached from the nanotubes during oxidation, the electrode surface after oxidation would not contain CNTs because the CNTs alone, without the attached PVF layers, cannot be deposited. Therefore, the successful codeposition of CNTs and PVF would suggest stable attachment of PVF to CNTs during redox transformation. Figure 5c (also Figure S12c) shows that, when the PVF/CNT dispersion was subjected to the electrochemical oxidation, a solid film that was morphologically different from the pure polymer film (Figure 5a and Figure S12a) was formed on the electrode

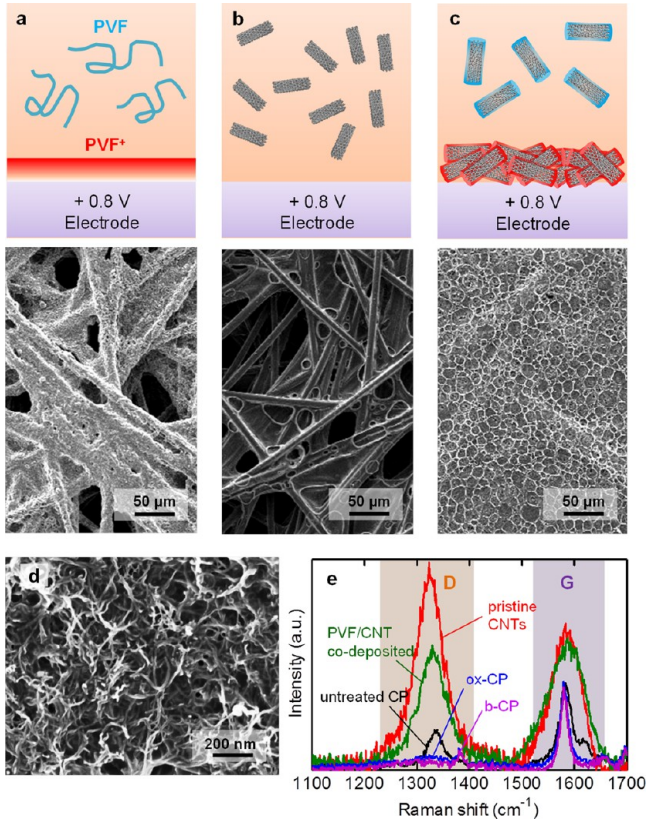

Figure 5. Electrochemical oxidation. (a–c) Schematic representations of the electrochemical oxidation processes and corresponding SEM images of the electrode surfaces obtained from different solutions containing (a) PVF, (b) pristine MWCNTs, and (c) PVF/MWCNT complexes. Higher magnification images are shown in Figure S13. (d) A HR-SEM image of the surface of the PVF/MWCNT codeposited electrode. (e) Raman spectra of the untreated carbon paper (CP) electrode (black), the oxidation-treated CP electrode in a control solution with only chloroform and background electrolyte (ox-CP, blue), the CP electrode treated in a MWCNT/chloroform solution as shown in (b) (b-CP, purple), the PVF/MWCNT codeposited CP electrode (green), and the pristine MWCNTs (red).

surface. A high-resolution SEM (HR-SEM) image of this solid film reveals clearly the interconnected CNTs distributed uniformly in the polymer film (Figure 5d). Notably, this successful deposition of nanotubes also indicates a novel, convenient route toward preparation of CNT-functionalized surfaces through the use of a redox-responsive nanotube dispersant.

Raman spectroscopy was used to confirm the presence of MWCNTs on the CP electrode treated by electrochemical oxidation in the PVF/CNT dispersion. Different types of carbonaceous materials can be easily distinguished by the R_I values obtained from their Raman spectra (Figure 5e), which is defined as the intensity of the D-band around 1330 cm^{-1} divided by that of the G-band around 1585 cm^{-1}.[59] The pristine CP electrode had an R_I value of 0.5. After oxidation at 0.8 V for 30 min in a control solution (i.e., chloroform with only the background electrolyte), the D-band disappeared and the oxidation-treated CP electrode had an R_I value of zero (see the spectrum in Figure 5e labeled as "ox-CP"). One possible explanation for this could be that the edge-plane sites of the carbon paper were affected by the electrochemical oxidation process, and the D-band intensity of carbonaceous materials is

dx.doi.org/10.1021/la401440w | Langmuir 2013, 29, 9626–9634

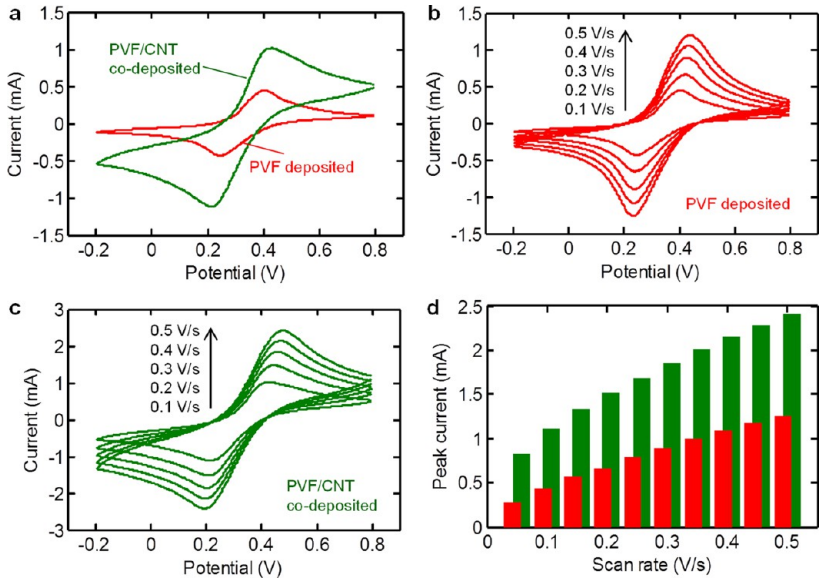

Figure 6. Cyclic voltammetric analysis. (a) Cyclic voltammograms (CVs) obtained on a PVF deposited electrode and a PVF/MWCNT codeposited electrode in 0.5 M $NaClO_4$ aqueous solution at a scan rate of 0.1 V s^{-1}. The quantities of deposited PVF in both cases are the same. (b) CV curves at various scan rates obtained on the PVF deposited electrode. (c) CV curves at various scan rates obtained on the PVF/MWCNT codeposited electrode. (d) Comparison of the anodic peak currents from CVs obtained on the PVF deposited electrode (red) with the current values obtained on the PVF/MWCNT codeposited electrode (green).

very sensitive to the density of the edge-plane sites. The CP electrode electrochemically treated in a MWCNT/chloroform dispersion, representing the deposition process shown in Figure 5b, had a Raman spectrum (labeled as "b-CP") that was very similar to that of ox-CP. This further confirms that this electrode (b-CP) did not have any CNTs deposited, in accord with the SEM image in Figure 5b. In contrast, the PVF/CNT codeposited CP electrode exhibited a pronounced D peak and an increased R_I value (0.9), compared to those of the pristine CP, ox-CP, and b-CP. This was due to the deposited nanotubes, which had a strong D peak and a high R_I value of 1.4 in their pristine state. It should be noted that the Raman spectrum for the PVF/CNT codeposited CP electrode had two contributions: one from the deposited CNTs and the other from the oxidized CP substrate. Thus, the R_I value for the PVF/CNT codeposited CP electrode (0.9) was in between the value for pristine CNTs (1.4) and the value of approximately 0 for the oxidized CP substrate (see "ox-CP" in Figure 5e). For calculation of the R_I values, see SI section S1.10.

The incorporation of nanotubes into the PVF film was also verified by comparing the current response of the PVF/CNT codeposited electrode with that of the PVF deposited electrode. The current responses were measured by CV in 0.5 M $NaClO_4$ aqueous solution (for experimental details, see SI section S1.11). The quantities of PVF deposited on both electrodes were kept the same by controlling the charge passed on the electrode surfaces at 80 mC during electrochemical deposition. As shown in Figure 6a, the CV curve of the PVF/CNT codeposited electrode obtained at a scan rate of 0.1 V s^{-1} exhibited an anodic peak current of 1.0 mA at 0.43 V and a cathodic peak current of −1.1 mA at 0.21 V, whereas the CV curve of the PVF-deposited electrode obtained at the same scan rate showed an anodic peak current of 0.4 mA at 0.41 V and a cathodic peak current of −0.4 mA at 0.24 V. The peak positions are in good agreement with the reported values for PVF.[60] This confirms the successful deposition of PVF onto the carbon paper electrodes in both cases and complements the observed morphological changes in the SEM images (Figure 5a,c). More importantly, the peak currents of the PVF/CNT codeposited electrode were amplified to about twice the values obtained on the PVF deposited electrode. This increase in the current response was attributed to the incorporation of highly conductive nanotubes into the PVF film, which may facilitate electron transport throughout the polymer matrix and therefore allow more efficient redox transformation of ferrocene. The CV curves obtained at various scan rates (Figure 6b,c) showed that both electrodes exhibited well-defined voltammetric responses of PVF; the anodic peak currents at all scan rates obtained on the PVF/CNT codeposited electrode were significantly higher than the values obtained on the PVF deposited electrode (Figure 6d).

CONCLUSION

In summary, we show that PVF can noncovalently disperse CNTs to individualized tubes with extremely high concentrations in organic solvents. This offers new opportunities for the design of new noncovalent-type ferrocene-based dispersants that do not rely on any conjugated or ionic moiety and expands CNT technologies in nonaqueous media such as CNT–polymer composites and organic liquid-based optical limiters. We also demonstrate that PVF's redox-tunable affinity for organic solvents, together with its stable attachment to the nanotubes during redox transformation, allows for controllable dispersion and aggregation of nanotubes, opening up new avenues for tailoring CNT dispersion behavior via external stimuli, with potential applications in nanotube-based responsive systems such as switching devices. This behavior further provides an electrochemically controlled approach to generating CNT-functionalized surfaces of different shapes, which can be used for sensing and catalysis. Moreover, since ferrocene is a well-known redox mediator for biosensing and can undergo reversible and fast redox reactions, the PVF/CNT hybrid system, with its greatly enhanced current response, can be

dx.doi.org/10.1021/la401440w | Langmuir 2013, 29, 9626–9634

potentially used for high-performance biosensor and pseudo-capacitive energy storage devices.

■ ASSOCIATED CONTENT

Supporting Information

Additional experimental details, improved dispersion quality of CNTs in polystyrene by PVF, PVF's redox-switchable affinity for chloroform, and supplementary figures. This material is available free of charge via the Internet at http://pubs.acs.org.

■ AUTHOR INFORMATION

Corresponding Author

*E-mail: tahatton@mit.edu (T.A.H.); rutledge@mit.edu (G.C.R.).

Notes

The authors declare no competing financial interest.

■ ACKNOWLEDGMENTS

We gratefully acknowledge the financial support by the U.S. Department of Energy.

■ REFERENCES

(1) Baughman, R. H.; Zakhidov, A. A.; de Heer, W. A. Carbon nanotubes - the route toward applications. *Science* **2002**, *297*, 787.

(2) Tasis, D.; Tagmatarchis, N.; Bianco, A.; Prato, M. Chemistry of carbon nanotubes. *Chem Rev* **2006**, *106*, 1105.

(3) Premkumar, T.; Mezzenga, R.; Geckeler, K. E. Carbon nanotubes in the liquid phase: addressing the issue of dispersion. *Small* **2012**, *8*, 1299.

(4) Kim, S. W.; Kim, T.; Kim, Y. S.; Choi, H. S.; Lim, H. J.; Yang, S. J.; Park, C. R. Surface modifications for the effective dispersion of carbon nanotubes in solvents and polymers. *Carbon* **2012**, *50*, 3.

(5) Gigliotti, B.; Sakizzie, B.; Bethune, D. S.; Shelby, R. M.; Cha, J. N. Sequence-independent helical wrapping of singles-walled carbon nanotubes by long genomic DNA. *Nano Lett.* **2006**, *6*, 159.

(6) Lu, G.; Maragakis, P.; Kaxiras, E. Carbon nanotube interaction with DNA. *Nano Lett.* **2005**, *5*, 897.

(7) Kam, N. W. S.; Liu, Z. A.; Dai, H. J. Carbon nanotubes as intracellular transporters for proteins and DNA: An investigation of the uptake mechanism and pathway. *Angew. Chem., Int. Ed.* **2006**, *45*, 577.

(8) Zheng, M.; Semke, E. D. Enrichment of single chirality carbon nanotubes. *J. Am. Chem. Soc.* **2007**, *129*, 6084.

(9) Sgobba, V.; Rahman, G. M. A.; Guldi, D. M.; Jux, N.; Campidelli, S.; Prato, M. Supramolecular assemblies of different carbon nanotubes for photoconversion processes. *Adv. Mater.* **2006**, *18*, 2264.

(10) Ehli, C.; Rahman, G. M. A.; Jux, N.; Balbinot, D.; Guldi, D. M.; Paolucci, F.; Marcaccio, M.; Paolucci, D.; Melle-Franco, M.; Zerbetto, F.; Campidelli, S.; Prato, M. Interactions in single wall carbon nanotubes/pyrene/porphyrin nanohybrids. *J. Am. Chem. Soc.* **2006**, *128*, 11222.

(11) Guldi, D. M.; Rahman, G. M. A.; Prato, M.; Jux, N.; Qin, S. H.; Ford, W. Single-wall carbon nanotubes as integrative building blocks for solar-energy conversion. *Angew. Chem., Int. Ed.* **2005**, *44*, 2015.

(12) Peng, X.; Komatsu, N.; Bhattacharya, S.; Shimawaki, T.; Aonuma, S.; Kimura, T.; Osuka, A. Optically active single-walled carbon nanotubes. *Nat. Nanotechnol.* **2007**, *2*, 361.

(13) Cheng, F. Y.; Zhang, S.; Adronov, A.; Echegoyen, L.; Diederich, F. Triply fused Zn-II-porphyrin oligomers: Synthesis, properties, and supramolecular interactions with single-walled carbon nanotubes (SWNTs). *Chem.—Eur. J.* **2006**, *12*, 6062.

(14) Guldi, D. M.; Taieb, H.; Rahman, G. M. A.; Tagmatarchis, N.; Prato, M. Novel photoactive single-walled carbon nanotube-porphyrin polymer wraps: Efficient and long-lived intracomplex charge separation. *Adv. Mater.* **2005**, *17*, 871.

(15) Goh, R. G. S.; Motta, N.; Bell, J. M.; Waclawik, E. R.: Effects of substrate curvature on the adsorption of poly(3-hexylthiophene) on single-walled carbon nanotubes. *Appl. Phys. Lett.* **2006**, *88*.

(16) Ikeda, A.; Nobusawa, K.; Hamano, T.; Kikuchi, J. Single-walled carbon nanotubes template the one-dimensional ordering of a polythiophene derivative. *Org. Lett.* **2006**, *8*, 5489.

(17) Mandal, A.; Nandi, A. K. Noncovalent functionalization of multiwalled carbon nanotube by a polythiophene-based compatibilizer: reinforcement and conductivity improvement in poly(vinylidene fluoride) films. *J. Phys. Chem. C* **2012**, *116*, 9360.

(18) Lee, H. W.; Yoon, Y.; Park, S.; Oh, J. H.; Hong, S.; Liyanage, L. S.; Wang, H. L.; Morishita, S.; Patil, N.; Park, Y. J.; Park, J. J.; Spakowitz, A.; Galli, G.; Gygi, F.; Wong, P. H. S.; Tok, J. B. H.; Kim, J. M.; Bao, Z. A.: Selective dispersion of high purity semiconducting single-walled carbon nanotubes with regioregular poly(3-alkylthiophene)s. *Nat. Commun.* **2011**, *2*.

(19) Star, A.; Stoddart, J. F.; Steuerman, D.; Diehl, M.; Boukai, A.; Wong, E. W.; Yang, X.; Chung, S. W.; Choi, H.; Heath, J. R. Preparation and properties of polymer-wrapped single-walled carbon nanotubes. *Angew. Chem., Int. Ed.* **2001**, *40*, 1721.

(20) Dalton, A. B.; Stephan, C.; Coleman, J. N.; McCarthy, B.; Ajayan, P. M.; Lefrant, S.; Bernier, P.; Blau, W. J.; Byrne, H. J. Selective interaction of a semiconjugated organic polymer with single-wall nanotubes. *J. Phys. Chem. B* **2000**, *104*, 10012.

(21) Chen, J.; Liu, H. Y.; Weimer, W. A.; Halls, M. D.; Waldeck, D. H.; Walker, G. C. Noncovalent engineering of carbon nanotube surfaces by rigid, functional conjugated polymers. *J. Am. Chem. Soc.* **2002**, *124*, 9034.

(22) Rice, N. A.; Soper, K.; Zhou, N. Z.; Merschrod, E.; Zhao, Y. M. Dispersing as-prepared single-walled carbon nanotube powders with linear conjugated polymers. *Chem. Commun.* **2006**, 4937.

(23) Zou, J. H.; Liu, L. W.; Chen, H.; Khondaker, S. I.; McCullough, R. D.; Huo, Q.; Zhai, L. Dispersion of pristine carbon nanotubes using conjugated block copolymers. *Adv. Mater.* **2008**, *20*, 2055.

(24) Maeda, Y.; Kimura, S.; Hirashima, Y.; Kanda, M.; Lian, Y. F.; Wakahara, T.; Akasaka, T.; Hasegawa, T.; Tokumoto, H.; Shimizu, T.; Kataura, H.; Miyauchi, Y.; Maruyama, S.; Kobayashi, K.; Nagase, S. Dispersion of single-walled carbon nanotube bundles in nonaqueous solution. *J. Phys. Chem. B* **2004**, *108*, 18395.

(25) Sabba, Y.; Thomas, E. L. High-concentration dispersion of single-wall carbon nanotubes. *Macromolecules* **2004**, *37*, 4815.

(26) Sun, G. X.; Chen, G. M.; Liu, J.; Yang, J. P.; Xie, J. Y.; Liu, Z. P.; Li, R.; Li, X. A facile gemini surfactant-improved dispersion of carbon nanotubes in polystyrene. *Polymer* **2009**, *50*, 5787.

(27) Lovell, C. S.; Wise, K. E.; Kim, J. W.; Lillehei, P. T.; Harrison, J. S.; Park, C. Thermodynamic approach to enhanced dispersion and physical properties in a carbon nanotube/polypeptide nanocomposite. *Polymer* **2009**, *50*, 1925.

(28) Zhang, Z. X.; Che, Y. K.; Smaldone, R. A.; Xu, M. A.; Bunes, B. R.; Moore, J. S.; Zang, L. Reversible dispersion and release of carbon nanotubes using foldable oligomers. *J. Am. Chem. Soc.* **2010**, *132*, 14113.

(29) Umeyama, T.; Kawabata, K.; Tezuka, N.; Matano, Y.; Miyato, Y.; Matsushige, K.; Tsujimoto, M.; Isoda, S.; Takano, M.; Imahori, H. Dispersion of carbon nanotubes by photo- and thermal-responsive polymers containing azobenzene unit in the backbone. *Chem. Commun.* **2010**, *46*, 5969.

(30) Zhao, W.; Liu, Y. T.; Feng, Q. P.; Xie, X. M.; Wang, X. H.; Ye, X. Y. Dispersion and noncovalent modification of multiwalled carbon nanotubes by various polystyrene-based polymers. *J. Appl. Polym. Sci.* **2008**, *109*, 3525.

(31) Deria, P.; Sinks, L. E.; Park, T. H.; Tomezsko, D. M.; Brukman, M. J.; Bonnell, D. A.; Therien, M. J. Phase transfer catalysts drive diverse organic solvent solubility of single-walled carbon nanotubes helically wrapped by ionic, semiconducting polymers. *Nano Lett.* **2010**, *10*, 4192.

(32) Chen, S. L.; Jiang, Y. G.; Wang, Z. Q.; Zhang, X.; Dai, L. M.; Smet, M. Light-controlled single-walled carbon nanotube dispersions in aqueous solution. *Langmuir* **2008**, *24*, 9233.

(33) Grunlan, J. C.; Liu, L.; Kim, Y. S. Tunable single-walled carbon nanotube microstructure in the liquid and solid states using poly(acrylic acid). *Nano Lett.* **2006**, *6*, 911.
(34) Nepal, D.; Geckeler, K. E. pH-sensitive dispersion and debundling of single-walled carbon nanotubes: Lysozyme as a tool. *Small* **2006**, *2*, 406.
(35) Wang, D.; Chen, L. W. Temperature and pH-responsive single-walled carbon nanotube dispersions. *Nano Lett.* **2007**, *7*, 1480.
(36) Etika, K. C.; Jochum, F. D.; Theato, P.; Grunlan, J. C. Temperature controlled dispersion of carbon nanotubes in water with pyrene-functionalized poly(N-cyclopropylacrylamide). *J. Am. Chem. Soc.* **2009**, *131*, 13598.
(37) Ding, Y.; Chen, S. L.; Xu, H. P.; Wang, Z. Q.; Zhang, X.; Ngo, T. H.; Smet, M. Reversible dispersion of single-walled carbon nanotubes based on a CO_2-responsive dispersant. *Langmuir* **2010**, *26*, 16667.
(38) Fujishige, S.; Kubota, K.; Ando, I. Phase-transition of aqueous-solutions of poly(N-Isopropylacrylamide) and poly(N-Isopropylmethacrylamide). *J. Phys. Chem.* **1989**, *93*, 3311.
(39) Akhoury, A.; Bromberg, L.; Hatton, T. A. Redox-responsive gels with tunable hydrophobicity for controlled solubilization and release of organics. *ACS Appl. Mater. Interfaces* **2011**, *3*, 1167.
(40) Guldi, D. M.; Marcaccio, M.; Paolucci, D.; Paolucci, F.; Tagmatarchis, N.; Tasis, D.; Vazquez, E.; Prato, M. Single-wall carbon nanotube-ferrocene nanohybrids: Observing intramolecular electron transfer in functionalized SWNTs. *Angew. Chem., Int. Ed.* **2003**, *42*, 4206.
(41) Kandimalla, V. B.; Tripathi, V. S.; Ju, H. X. A conductive ormosil encapsulated with ferrocene conjugate and multiwall carbon nanotubes for biosensing application. *Biomaterials* **2006**, *27*, 1167.
(42) Callegari, A.; Marcaccio, M.; Paolucci, D.; Paolucci, F.; Tagmatarchis, N.; Tasis, D.; Vazquez, E.; Prato, M. Anion recognition by functionalized single wall carbon nanotubes. *Chem. Commun.* **2003**, 2576.
(43) Callegari, A.; Cosnier, S.; Marcaccio, M.; Paolucci, D.; Paolucci, F.; Georgakilas, V.; Tagmatarchis, N.; Vazquez, E.; Prato, M. Functionalised single wall carbon nanotubes/polypyrrole composites for the preparation of amperometric glucose biosensors. *J. Mater. Chem.* **2004**, *14*, 807.
(44) Huang, X. J.; Im, H. S.; Lee, D. H.; Kim, H. S.; Choi, Y. K. Ferrocene functionalized single-walled carbon nanotube bundles. Hybrid interdigitated construction film for L-glutamate detection. *J. Phys. Chem. C* **2007**, *111*, 1200.
(45) Jiao, S. F.; Li, M. G.; Wang, C.; Chen, D. L.; Fang, B. Fabrication of Fc-SWNTs modified glassy carbon electrode for selective and sensitive determination of dopamine in the presence of AA and UA. *Electrochim. Acta* **2007**, *52*, 5939.
(46) Yang, X. Y.; Lu, Y. H.; Ma, Y. F.; Li, Y. J.; Du, F.; Chen, Y. S. Noncovalent nanohybrid of ferrocene with single-walled carbon nanotubes and its enhanced electrochemical property. *Chem. Phys. Lett.* **2006**, *420*, 416.
(47) Yang, X. Y.; Lu, Y. H.; Ma, Y. F.; Liu, Z. F.; Du, F.; Chen, Y. S. DNA electrochemical sensor based on an adduct of single-walled carbon nanotubes and ferrocene. *Biotechnol. Lett.* **2007**, *29*, 1775.
(48) Yan, Y. H.; Cui, J. A.; Potschke, P.; Voit, B. Dispersion of pristine single-walled carbon nanotubes using pyrene-capped polystyrene and its application for preparation of polystyrene matrix composites. *Carbon* **2010**, *48*, 2603.
(49) Wang, J.; Fruchtl, D.; Sun, Z. Y.; Coleman, J. N.; Blau, W. J. Control of optical limiting of carbon nanotube dispersions by changing solvent parameters. *J. Phys. Chem. C* **2010**, *114*, 6148.
(50) Coleman, J. N.; Khan, U.; Gun'ko, Y. K. Mechanical reinforcement of polymers using carbon nanotubes. *Adv. Mater.* **2006**, *18*, 689.
(51) Guan, L. H.; Shi, Z. J.; Li, M. X.; Gu, Z. N. Ferrocene-filled single-walled carbon nanotubes. *Carbon* **2005**, *43*, 2780.
(52) Kim, K. K.; Yoon, S. M.; Choi, J. Y.; Lee, J.; Kim, B. K.; Kim, J. M.; Lee, J. H.; Paik, U.; Park, M. H.; Yang, C. W.; An, K. H.; Chung, Y. S.; Lee, Y. H. Design of dispersants for the dispersion of carbon nanotubes in an organic solvent. *Adv. Funct. Mater.* **2007**, *17*, 1775.
(53) Costanzo, G. D.; Ledesma, S.; Mondragon, M.; Goyanes, S. Stable solutions of multiwalled carbon nanotubes using an azobenzene dye. *J. Phys. Chem. C* **2010**, *114*, 14347.
(54) Nguyen, M. T.; Diaz, A. F.; Dementev, V. V.; Pannell, K. H. High-molecular-weight poly(ferrocenediyl silanes) - synthesis and electrochemistry of $[\text{-}(C_5H_4)Fe(C_5H_4)SiR^{2-}]N$, R = Me, Et, N-Bu, N-Hex. *Chem. Mater.* **1993**, *5*, 1389.
(55) Evans, D. H. One-electron and two-electron transfers in electrochemistry and homogeneous solution reactions. *Chem. Rev.* **2008**, *108*, 2113.
(56) Manners, I. *Synthetic Metal-Containing Polymers*; Wiley-VCH: Weinheim, 2004.
(57) Wang, Z. P.; Mohwald, H.; Gao, C. Y. Preparation and redox-controlled reversible response of ferrocene-modified poly(allylamine hydrochloride) microcapsules. *Langmuir* **2011**, *27*, 1286.
(58) Sen, S.; Gok, A. U.; Gulce, H.; Aldissi, M. Synthesis and characterization of polyvinylferrocene/polypyrrole composites. *J. Macromol. Sci., Part A* **2008**, *45*, 485.
(59) Pimenta, M. A.; Dresselhaus, G.; Dresselhaus, M. S.; Cancado, L. G.; Jorio, A.; Saito, R. Studying disorder in graphite-based systems by Raman spectroscopy. *Phys. Chem. Chem. Phys.* **2007**, *9*, 1276.
(60) Glidle, A.; Hillman, A. R.; Rydeo, K. S.; Smith, E. L.; Cooper, J.; Gadegaard, N.; Webster, J. R. P.; Dalgliesh, R.; Cubitt, R. Use of neutron reflectivity to measure the dynamics of solvation and structural changes in polyvinylferrocene films during electrochemically controlled redox cycling. *Langmuir* **2009**, *25*, 4093.